HYDROLOGICAL PROCESSES
Hydrol. Process. **16**, 1645–1662 (2002)
Published online in Wiley InterScience (www.interscience.wiley.com). DOI: 10.1002/hyp.1051

Assimilating remote sensing data in a surface flux–soil moisture model

William L. Crosson,[1]* Charles A. Laymon,[1] Ramarao Inguva[2] and Marius P. Schamschula[3]

[1] *Institute for Global Change Research and Education,† Huntsville, AL, USA*
[2] *East–West Enterprises, Inc., Huntsville, AL, USA*
[3] *Center for Applied Optical Sciences, Center for Hydrology, Soil Climatology and Remote Sensing, Alabama A&M University, Normal, AL, USA*

Abstract:

A key state variable in land surface–atmosphere interactions is soil moisture, which affects surface energy fluxes, runoff and the radiation balance. Soil moisture modelling relies on parameter estimates that are inadequately measured at the necessarily fine model scales. Hence, model soil moisture estimates are imperfect and often drift away from reality through simulation time. Because of its spatial and temporal nature, remote sensing holds great promise for soil moisture estimation. Much success has been attained in recent years in soil moisture estimation using passive and active microwave sensors, but progress has been slow. One reason for this is the scale disparity between remote sensing data resolution and the hydrologic process scale. Other impediments include vegetation cover and microwave penetration depth. As a result, currently there is no comprehensive method for assimilating remote soil moisture observations within a surface hydrology model at watershed or larger scales.

This paper describes a measurement–modelling system for estimating the three-dimensional soil moisture distribution, incorporating remote microwave observations, a surface flux–soil moisture model, a radiative transfer model and Kalman filtering. The surface model, driven by meteorological observations, estimates the vertical and lateral distribution of water. Based on the model soil moisture profiles, microwave brightness temperatures are estimated using the radiative transfer model. A Kalman filter is then applied using modelled and observed brightness temperatures to update the model soil moisture profile.

The modelling system has been applied using data from the Southern Great Plains 1997 field experiment. In the presence of highly inaccurate rainfall input, assimilation of remote microwave data results in better agreement with observed soil moisture. Without assimilation, it was seen that the model near-surface soil moisture reached a minimum that was higher than observed, resulting in substantial errors during very dry conditions. Updating moisture profiles daily with remotely sensed brightness temperatures reduced but did not eliminate this bias. Copyright © 2002 John Wiley & Sons, Ltd.

KEY WORDS soil moisture; data assimilation; microwave brightness temperature; remote sensing

INTRODUCTION

Background and motivation

Despite a need in many earth science disciplines for soil moisture information, large-scale continuous soil moisture measurements are not possible today. The accuracy of soil moisture estimated by hydrology models depends on the model physics and the number and configuration of soil layers, as well as the accuracy and the temporal and spatial nature of the input data. Because modelled soil moisture estimates are temporally correlated, model estimates tend to deviate systematically from reality in the absence of new measurements.

* Correspondence to: William L. Crosson, Global Hydrology and Climate Center, National Space Science & Technology Center, 320 Sparkman Dr, Huntsville, AL 35805, USA. E-mail: bill.crosson@nstc.nasa.gov
† IGCRE is jointly operated by the University of Alabama in Huntsville and the Universities Space Research Association.

Received 24 November 1998
Accepted 1 March 2000

Meteorological and hydrological observations or predictions are typically available at 6–24 h intervals and are subject to significant errors. This is especially true for radar or raingauge estimates of precipitation, which is the primary control on soil moisture. Such long sampling intervals and uncertainties can produce unacceptable errors in soil moisture. Utilization of remote sensing data directly in a model may potentially improve model soil moisture estimates at high spatial and temporal resolutions.

Remote sensing of soil moisture from space is advantageous because of its spatial coverage and temporal continuity. Research in soil moisture remote sensing began in the mid 1970s (Eagleman and Lin, 1976; Njoku and Kong, 1977). Recent advances in remote sensing have shown that soil moisture, or at least 'surface wetness', can be measured by several methods. Quantitative measurements of surface layer soil moisture have been most successful using both passive and active remote sensing in the microwave region. Early attempts to measure soil moisture from space using passive microwave sensors were hindered by what is now considered a less-than-optimal frequency and/or coarse spatial resolution. The lowest frequency of the Scanning Multichannel Microwave Radiometer (SMMR), launched in 1978, was 6·6 GHz and yielded a resolution of about 140 km. The lowest frequency of the Special Sensor Microwave Imager (SSM/I), launched in 1987, is 19·3 GHz and has a resolution of about 40 km. In addition to problems of spatial resolution, attenuation of microwave radiation in the presence of even small amounts of vegetation becomes a problem at relatively high frequencies, such as the 19·3 GHz SSM/I channel. Two new radiometers may offer some hope for satellite remote sensing of surface wetness. The Tropical Rainfall Measuring Mission (TRMM) Microwave Imager (TMI), launched in 1997, has a ground resolution of about 45 km for its 10·65 GHz channel. The Advanced Microwave Scanning Radiometer (AMSR) to be launched on NASA's Earth Observing System (EOS) Aqua satellite and on the Japanese Advanced Earth Observing Satellites-II (ADEOS-II) in 2002 has a resolution of 56 km at 6·9 GHz. However, the aforementioned resolution and vegetation problems may impede progress toward estimating soil moisture with TMI and AMSR.

Existing space-borne synthetic aperture radars (SARs) have shown some potential to detect surface wetness. These instruments operate in the C-band (European Remote Sensing, ERS-1, and the Canadian RADARSAT) and L-band (Japanese Earth Resources Satellite, JERS-1). The advantage of radar systems is their much higher resolution relative to passive microwave systems, but they are currently hampered by the lack of a good algorithm that is based on a single frequency and single polarization. In addition, their repeat frequency is generally low (about 40 days). RADARSAT can achieve a repeat cycle as little as 3 days with its SCANSAR mode, but this is not practical on a global scale.

Early modelling studies showed that even infrequent soil moisture measurements can lead to better soil water budget estimates. Benard *et al*. (1981) demonstrated that evaporation could be modelled very accurately with the contribution of surface moisture measurements every 3 days. Prevot *et al*. (1984) continued this work and showed that the soil water balance could be determined with equal accuracy using remotely sensed surface soil moisture estimates substituted for *in situ* observations. Smith and Newton (1983) developed a soil water simulation model that utilized remotely sensed data to predict profile moisture.

Recent investigations have focused on the assimilation of remote sensing data in hydrologic models for the purpose of improving soil moisture estimation. Entekhabi *et al*. (1994) demonstrated in a theoretical study the potential for assimilating microwave data using a Kalman filter. This scheme was tested using daily microwave observations over an 8 day period, as well as through a 4 month simulation in which simulated microwave 'observations' were used to update soil moisture at 3 day intervals (Galantowicz *et al*., 1999). In this study, rainfall information was withheld from the hydrologic model, and it was found that the assimilation of remotely sensed estimates resulted in excellent soil moisture retrievals, as long as the soil properties were known with good accuracy. Li *et al*. (1998) performed a feasibility study in which intermittent *in situ* soil moisture measurements served as a proxy for remote sensing observations. Their approach was to adjust iteratively the soil hydraulic conductivity and evaporative parameters to force the modelled near-surface soil moisture to match measurements better. They found that by doing so the agreement between measured and modelled soil moisture improved not only in the surface layer but in the root zone as well. Houser *et al*. (1998), using a distributed hydrologic model, applied various data assimilation methods to simulate soil moisture fields

based on incomplete remote sensing coverage, but did not address the disparate spatial resolutions of remote observations and surface models. They concluded that assimilation schemes of low to moderate complexity performed nearly as well as more complex ones, and with a smaller computational burden.

Despite the potential, the hydrologic community has been slow to embrace soil moisture remote sensing. Algorithm development is complicated by the need for surface roughness and vegetation corrections, which are based on empirical relationships developed from limited data. Laymon *et al*. (1999) found that typical errors in vegetation water content may result in soil moisture retrieval errors of up to 5% volumetric water content for typical moisture conditions, and even higher for very wet soils. Errors in soil moisture related to uncertainties in soil texture and surface roughness were seen to be almost as large. Another problem is that satellites can only provide measurements every few days or so under the best orbital circumstances. Perhaps the biggest challenge stems from the resolution of the remote sensing data sets, which is inconsistent with the scale of the hydrologic processes of interest. The 45–56 km resolution of current satellite-borne passive microwave sensors (TMI, AMSR) may be useful for supplying moisture estimates to numerical weather prediction models, but this is too coarse for most hydrologic applications. L-band (1–3 GHz) observations are now deemed optimal for soil moisture detection (Jackson and Schmugge, 1989), but they are limited to the upper few centimetres of soil (Engman and Chauhan, 1995; Jackson *et al*., 1997). The Electronically Steered Thinned Array Radiometer (ESTAR), a 1·4 GHz aircraft-based instrument, has shown promise for soil moisture determination (Jackson *et al*., 1995). Initiatives are underway to develop an L-band instrument for space to provide soil moisture estimates at 30 km resolution with a repeat frequency of 3 days or less, but such an instrument will not be deployed for several years.

Scientific objective

The objective of this research is to apply a Kalman filter-based method for assimilating remotely sensed soil moisture estimates into a spatially distributed soil moisture model. This research addresses an important current issue: how useful are remotely sensed data in estimating soil moisture and how can they be applied in a way that minimizes their inherently deficient spatial and temporal resolutions? A Kalman filter provides an optimal solution based on both measurements and model estimates. This approach has the advantage of coupling the space–time continuity of a surface model with intermittent remote observations in a framework that balances model and measurement uncertainties. This paper describes a method for applying remote sensing data to update soil moisture estimates in a spatially distributed land surface model, and is similar to that of Entekhabi *et al*. (1994). The results presented herein pertain to point-scale testing of the modelling scheme using data from the Southern Great Plains 1997 (SGP97) hydrology experiment (Jackson *et al*., 1999). In the future we will extend the approach to address the more challenging problem of spatially distributed implementation using SGP97 observations.

MODEL FRAMEWORK AND APPLICATION

Overview

The diurnal cycle and spatial pattern of the soil moisture profile can be well represented by a land surface hydrology model, but these estimates may deviate from reality during long numerical simulations. Presumably, updating a model with remotely sensed soil moisture estimates would improve its performance. The framework used here for estimating the spatial nature of the soil moisture profile is represented in Figure 1. The starting point of the process is indicated on the left side of Figure 1, where a land surface hydrology model (see next section) is initialized with soil moisture profile information. At times when remotely sensed brightness temperatures are available (right side), model moisture profiles are used as input to the forward radiative transfer model, which is applied to produce brightness temperatures for a set of microwave frequencies on the model grid. Using modelled and remotely sensed brightness temperature estimates, a Kalman filter is applied

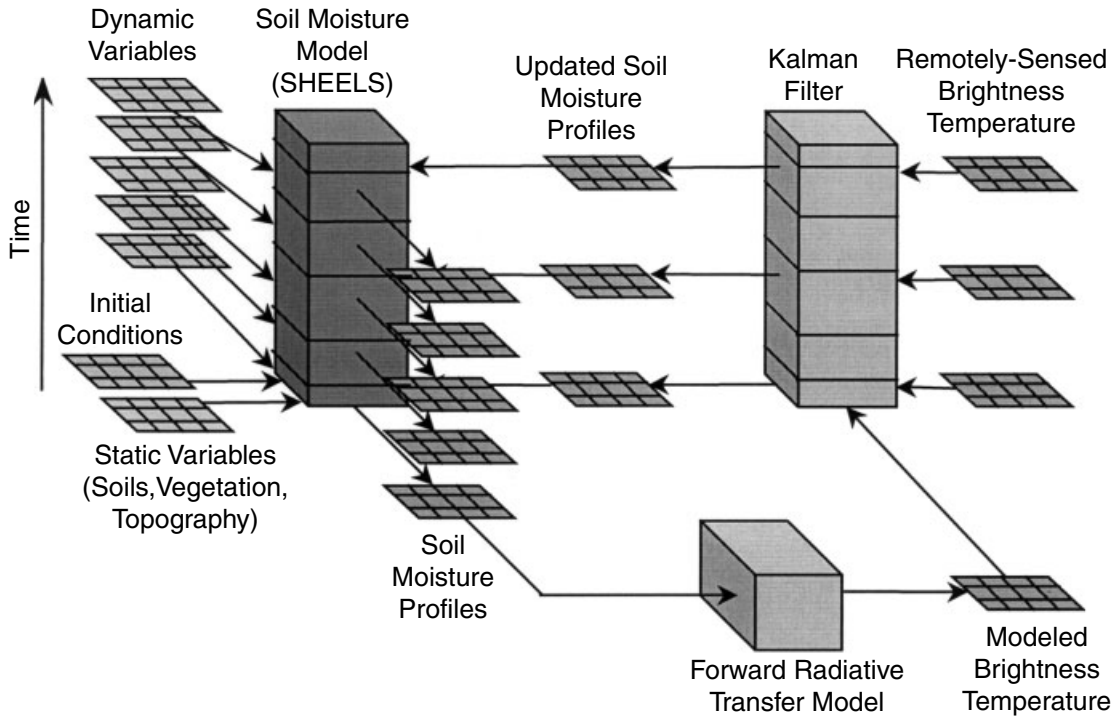

Figure 1. Schematic representation of the model–remote sensing soil moisture estimation scheme. Time is represented by the vertical dimension. Models or algorithms are represented by cubical elements, and their inputs and outputs are shown as two-dimensional grids

on the model grid to nudge model estimates toward the measurements. The resulting soil moisture profiles are then used to update the model, which is run until remote data are again available. An advantage to this system is that measured brightness temperatures are used directly to update soil moisture, obviating the need for an inverse radiative transfer model.

Models

Simulator for hydrology and energy exchange at the land surface (SHEELS). The land surface flux–soil moisture model used in this study is SHEELS. The physics of SHEELS are based on the biosphere–atmosphere transfer scheme (BATS) of Dickinson *et al.* (1993). SHEELS has retained the treatment of vegetation properties and the surface flux parameterizations of BATS. All relevant hydrologic and energy processes are modelled to determine moisture in each soil layer. Formulations of variables such as surface energy fluxes and temperatures are similar to those in an earlier version of the model (Smith *et al.*, 1993).

Sub-surface hydrologic processes in SHEELS differ significantly from BATS. The nested three-layer approach of BATS has been converted to a discrete layer configuration in SHEELS, in which the number and depth of layers are flexible. This permits higher vertical resolution near the surface where temperature and moisture gradients are large, and is compatible with remotely sensed moisture data. The vertical soil water dynamics algorithm has been modified following the Darcy flow approach of the soil hydrology model (SHM; Capehart and Carlson, 1994). Also, a lateral sub-surface flow component has been added. Together, these modules estimate the three-dimensional diffusive and gravitational soil water fluxes. Dynamic time stepping based on soil moisture has been introduced in these algorithms to maximize computational efficiency while satisfying numerical stability criteria.

SHEELS is driven by seven atmospheric forcing variables: air temperature, relative humidity, atmospheric pressure, incident solar and infrared radiative fluxes, wind speed and precipitation. Meteorological input

variables may be spatially distributed or uniform, depending on the scale of the model domain. SHEELS also requires spatially distributed soil properties, including saturated hydraulic conductivity, saturated matric potential, rooting depth, porosity, and wilting point. Required vegetation properties include canopy height, fractional vegetation cover, leaf area index, minimum stomatal resistance, and reflectance properties. Values for these soil and vegetation parameters and the methods used to obtain them are given in Table I.

The output of SHEELS consists primarily of surface energy fluxes and associated state variables describing temperatures and moisture conditions. SHEELS estimates volumetric water content at each time step for each soil layer. The layer thicknesses are model parameters and are defined to meet the needs of the application. For remote sensing studies in which the near-surface soil moisture is updated using microwave data, it is advisable to partition the upper 5–10 cm soil depth into layers of approximately 1–2 cm thickness. This permits a detailed characterization of the near-surface profile, and is particularly important when assimilating microwave observations at multiple frequencies, since each frequency gives information about a different soil depth. In this study the soil layer thickness is 2 cm.

Surface or skin temperature is determined in SHEELS based on the energy balance of the uppermost soil layer (2 cm), a thinner layer than the upper layer in BATS. The SHEELS skin temperature is thus more consistent with remotely sensed surface temperature. Canopy temperature is calculated from the vegetation energy budget, and is constrained using air temperature in order to prevent the 'runaway effect' in which canopy temperature becomes unrealistically high (Toby Carlson, personal communication).

The temporal change in soil moisture content in each of the soil layers is determined in SHEELS by considering the contributions of infiltration, evaporation, transpiration, diffusion, and gravitational drainage. Surface runoff and ponded water are also calculated. Infiltration I is calculated using the Green–Ampt equation based on the amount of precipitation P reaching the soil surface directly or through the vegetation canopy P_{d}. Surface runoff R_{u} is based on local slope angle ϕ and infiltration excess:

$$R_{\mathrm{u}} = (P + P_{\mathrm{d}} - I)\sin\phi \tag{1}$$

The amount of water reaching the soil surface that does not run off or infiltrate is assumed to pond on the surface. The change in depth of water in soil layer i (d_i) due to water exchange with the atmosphere can be expressed as:

$$\partial d_i/\partial t = I_i - E_i - T_i \tag{2}$$

where I_i, E_i, and T_i are the amounts of infiltration, evaporation, and transpiration attributed to layer i. These terms are proportions of the total quantities I, E, and T, and are determined by applying weighting functions to specified contributing depths for each variable. For infiltration,

$$I_i = w_i^{\mathrm{I}} I \tag{3}$$

where weight w_i^{I} is the proportion of the total infiltration that is extracted from layer i, and is defined to decrease linearly from the surface downward:

$$w_i^{\mathrm{I}} = [\Delta z_i(1 - z_i/D_{\mathrm{I}})]/(D_{\mathrm{I}}/2) \tag{4}$$

D_{I} is a landcover type-dependent variable representing the depth over which infiltration is distributed within one model time step, Δz_i is the thickness of layer i and z_i is the depth at the middle of layer i.

The weighting functions for evaporation and transpiration are obtained in a similar manner, but are modified in proportion to the soil moisture content within each layer. This allows for more evapotranspiration to be extracted for wet layers than for drier layers relative to the underlying weighting function, which decreases from the surface downward. For evaporation,

$$E_i = w_i^{\mathrm{E}} E \tag{5}$$

Table I. Definitions, values and data sources for parameters used in the SHEELS, RTM, and Kalman filter models

Parameter definition	Value	Units	Data source
SHEELS			
Number of soil layers in upper zone	5	unitless	
Number of soil layers in root zone	10	unitless	
Number of soil layers in bottom zone	25	unitless	
Thickness of upper zone	100	mm	
Thickness of root zone	200	mm	
Thickness of bottom zone	500	mm	
Porosity of upper zone	0·48	unitless	Mohanty (2001)
Porosity of root zone	0·45	unitless	Mohanty (2001)
Porosity of bottom zone	0·42	unitless	Mohanty (2001)
Saturated hydraulic conductivity of upper zone	0·02	mm s^{-1}	Mohanty (2001)
Saturated hydraulic conductivity of root zone	0·001	mm s^{-1}	Mohanty (2001)
Saturated hydraulic conductivity of bottom zone	0·0003	mm s^{-1}	Mohanty (2001)
Clapp–Hornberger soil parameter	6·5	unitless	Model optimization
Saturated soil suction (negative matric potential)	150	mm	Dickinson *et al*. (1993)
Soil moisture at which transpiration ceases	0·25	fractional	Dickinson *et al*. (1993)
Soil depth for evaporation and infiltration	50	mm	Estimated
Leaf area index	0·5	unitless	Estimated from field observations
Canopy height	0·2	m	Mohanty (2001)
Fractional vegetation cover	0·2	unitless	Estimated from field observations
Minimum stomatal resistance	300	s m^{-1}	Dickinson *et al*. (1993)
Minimum canopy visible albedo	0·1	unitless	Dickinson *et al*. (1993)
Minimum canopy near-IR albedo	0·3	unitless	Dickinson *et al*. (1993)
RTM			
Microwave frequencies	1·413, 2·65	GHz	SLMR configuration
Radiometer look angle	15	degrees	SLMR configuration
Bound water content in soil	0·05	m^3 m^{-3}	Jackson and Schmugge (1989), Dobson *et al*. (1985)
Vegetation water content	0·2	kg m^{-2}	J. Judge, personal communication
B parameter in RTM vegetation correction	0·3	m^2 kg^{-1}	Jackson and Schmugge (1991)
Surface RMS roughness	0·3	cm	Estimated from field observations
Empirical coefficient in soil mixing model	0·65	unitless	Dobson *et al*. (1985)
Deep soil (10 m) temperature	291	K	Annual mean temperature
Kalman filter			
Initial soil moisture variance	0·0004		Estimated
Model system propagation error variance	0·0001	$(m^3\ m^{-3})^2$ day^{-1}	Estimated
Observation (T_B) error variance	9	K^2	Estimated

where:

$$w_i^{\mathrm{E}} = w_i^{\mathrm{I}}\theta_i / \sum \left(w_i^{\mathrm{I}}\theta_i\right) \tag{6}$$

and θ_i is the volumetric water content (proportion of porosity) for layer i. The summation is over soil layers extending to depth D_{I}. The effect of Equations (3)–(6) is that the amount of water extracted via transpiration is distributed to the bottom of the root zone, whereas infiltration and evaporation affect a shallower layer of depth D_{I}.

After the layer water depths are updated by applying Equation (2) to account for 'external' forcing (infiltration, evaporation, and transpiration), volumetric water contents for each layer are updated. If a layer exceeds its saturation point, infiltration is reduced so that the layer is just saturated, and the excess water is partitioned between runoff and ponding based in the local slope. After accounting for external controls, the internal three-dimensional soil water fluxes (diffusion and drainage) are then determined at each grid cell. The vertical fluxes are formulated using Darcy's law:

$$q_\theta = -K\,\partial\psi/\partial z - K \tag{7}$$

where q_θ is the vertical water flux, $K = K(\theta)$ is the hydraulic conductivity, and $\psi = \psi(\theta)$ is the hydraulic matric potential.

Applying mass continuity and expressing terms as functions of θ yields the diagnostic equation:

$$\partial\theta/\partial t = -(1/\mathrm{p})\;\partial q_\theta/\partial z = \partial/\partial z[D(\theta)\,\partial\theta/\partial z] + G(\theta)\partial\theta/\partial z \tag{8}$$

where $\mathrm{p} =$ porosity, $D(\theta) = K{\cdot}\partial\psi/\partial\theta$ is the diffusion coefficient, and $G(\theta) = \partial K/\partial\theta$ is the gravitational coefficient.

Equation (8) is solved in matrix form for each of the soil layers at the 'Darcy time step', which depends on θ and is calculated from the numerical stability criterion. The diffusion term is solved using the Crank–Nicholson numerical scheme, and the functions $\psi(\theta)$ and $K(\theta)$ are given by the empirical parameterizations of Clapp and Homberger (1978).

Because of the different time scales of vertical and lateral sub-surface flow, these processes are treated in separate modules in SHEELS. After the soil water contents have been adjusted to account for vertical soil water fluxes, lateral sub-surface flow is considered. Darcy flow is assumed in the x and y directions, with the elevation at each grid point used to determine the total hydraulic potential differences between grid cells. Stream channels and impermeable boundaries are defined and used to set lateral boundary conditions.

Forward radiative transfer model (RTM). The forward RTM is a coherent wave model (Njoku and Kong, 1977) developed for a stratified medium characterized by potentially complex soil moisture and temperature profiles. The model is based on the relationship between surface microwave brightness temperature and the physical surface temperature through the effective emissivity, which is strongly controlled by the soil moisture content. The model is used in this study to estimate brightness temperature at specified microwave frequencies. Required input variables to the RTM are surface temperature, vegetation water content, and soil moisture, temperature and density profiles. The moisture and temperature profiles are obtained from SHEELS output. Values of other model parameters are given in Table I.

The brightness temperature for horizontal polarization, T_{B_0} neglecting the effects of surface roughness and vegetation, is given by:

$$T_{B_0} = \frac{k}{\cos(\phi)} \int_0^\infty T(z)\varepsilon(z)\psi(z)^2 \mathrm{d}z \tag{9}$$

where k is the free space wavenumber ($= 2\pi/\lambda$, where λ is wavelength), ϕ is the observation angle from nadir, $T(z)$ is temperature at depth z below the surface, $\varepsilon(z)$ is the complex dielectric constant, and $\psi(z)$ is subject to:

$$\frac{\mathrm{d}^2\psi(z)}{\mathrm{d}z^2} + \left\{\varepsilon(z)k^2 - [k\sin(\phi)]^2\right\}\psi(z) = 0 \tag{10}$$

Although soil moisture does not appear explicitly in Equations (9) and (10), it comes into effect through its strong influence on the dielectric constant. For a non-uniform temperature profile, a direct solution of Equations (9) and (10) is not feasible. Therefore, the problem is reformulated into one consisting of a stratified soil having layers that are thin enough to be assumed of uniform temperature and dielectric constant. In so doing, the integral in Equation (9) is replaced by a summation that accurately estimates the integral provided the thickness of the layer is small compared with the wavelength (Njoku and Kong, 1977). In the current study, the summation is performed using 50 soil layers, the thicknesses of which are inversely proportional to wavelength.

The effect of surface roughness has been incorporated into the model using the statistical method of Choudhury *et al*. (1979), which treats the soil surface height as having a Gaussian distribution with variance σ^2. The microwave reflectance of a bare rough surface is thus given by:

$$R_{\mathrm{br}} = R_{\mathrm{o}} \exp(-4\sigma^2 k^2 \cos^2 \phi) \tag{11}$$

where R_{o} is the reflectivity of a bare smooth surface.

The effect of vegetation on microwave brightness temperature is considered using the formulation of Jackson and Schmugge (1991), in which the transmissivity γ of the vegetation layer is determined as a function of the optical depth τ:

$$\gamma^2 = \exp[-2\tau \sec(\phi)] \tag{12}$$

and the optical depth is parameterized in terms of the vegetation water content w_{v}:

$$\tau = b w_{\mathrm{v}} \tag{13}$$

where b is an empirical coefficient. In this study, we used a constant value of $w_{\mathrm{v}} = 0{\cdot}2$ kg m^{-2} based on measurements, and assumed $b = 0{\cdot}3$ from previous studies of short grass (Jackson and Schmugge, 1991). The vegetation transmissivity is then used to obtain the surface reflectance for a vegetated rough surface:

$$R_{\mathrm{vr}} = \gamma^2 R_{\mathrm{br}} \tag{14}$$

Combining Equations (11)–(14), the brightness temperature T_{B} for a vegetated rough surface can be expressed in terms of the surface temperature and the reflectivity of a bare smooth surface:

$$T_{\mathrm{B}} = (1 - R_{\mathrm{vr}}) T_{\mathrm{sfc}} \tag{15}$$

$$= [1 - \gamma^2 R_{\mathrm{o}} \exp(-4\sigma^2 k^2 \cos^2 \phi)] T_{\mathrm{sfc}} \tag{16}$$

We estimated from field observations that the standard deviation σ of surface height was approximately 0·3 cm. Inclusion of the roughness factor increases the L-band T_{B} up to 5 K for dry to moderately wet soils, but the effect is somewhat greater for wet soils.

Kalman filter soil moisture updating. Our method for assimilating remotely sensed data is built on the assumption that remote observations are available at irregular intervals of 1 day or longer. Between updates, soil moisture evolves through the system equations. If the dynamical system were deterministic, its evolution could be predicted exactly. This is not the case here due to uncertainties in model physics, parameters, and initial conditions. Instead, the state vector $\boldsymbol{X}(t)$ satisfies the stochastic equation:

$$\mathrm{d}[\boldsymbol{X}(t)]/\mathrm{d}t = F[\boldsymbol{X}(t)] + w(t) \tag{17}$$

and the observation vector $\boldsymbol{Z}$ at time t_k satisfies:

$$\boldsymbol{Z}_k = h_k[\boldsymbol{X}_k] + v_k \tag{18}$$

where h is the non-linear representation of the radiative transfer model. The noise components $w(t)$ and v_k are assumed to be independent Gaussian random variables with covariance matrices $\boldsymbol{P}_k$ and $\boldsymbol{R}_k$ respectively. This is a classic extended Kalman filter problem of a stochastic–dynamic non-linear system in which imperfect, intermittent observations are used to nudge the model state toward the observation (Brown and Hwang, 1992). The amount of nudging is given by the Kalman gain and is based on the relative uncertainties of the state and observation vectors and the difference between the vectors. In this study the state vector is defined as the volumetric soil moisture profile at 40 layers of equal thickness (2 cm) down to 0·8 m depth. In the current application, the observation vector contains L- and S-band brightness temperatures obtained from a ground-based radiometer system (see next section on point-scale testing).

In Equation (17), $F[\boldsymbol{X}]$ is a simplified (but non-linear) version of the total soil moisture tendency as formulated in SHEELS, representing diffusion and gravitational drainage of water and a simple evapotranspiration parameterization, but neglecting infiltration, as follows:

$$\partial\theta/\partial t = \partial/\partial z(K\,\partial\psi/\partial z) + \partial K/\partial z - \mathrm{ET} \tag{19}$$

where ET is the amount of water extracted by evapotranspiration, given for layer k in the Kalman filter algorithm by:

$$\mathrm{ET}_k = \mathrm{ET}_{\max} e_k \theta_k / \Delta z \tag{20}$$

where $\mathrm{ET}_{\max}$ is a maximum ET rate and e_k is the proportion of the total ET that is extracted from layer k, expressed in a form similar to w_i^{E} in Equation (6).

Because our problem involves the nonlinear system in Equation (17), we use the extended Kalman filter method, in which the solution is linearized about a reference state vector $\boldsymbol{X}^*$. Writing Equation (17) in finite difference form:

$$\boldsymbol{X}_{k+1} = \boldsymbol{\Phi}_k \boldsymbol{X}_k + \boldsymbol{\Gamma}_k \tag{21}$$

where

$$\boldsymbol{\Phi}_k = \boldsymbol{I} + \boldsymbol{J}\,\Delta t \tag{22}$$

$$\boldsymbol{\Gamma}_k = [F(\boldsymbol{X}^*) - \boldsymbol{J}\boldsymbol{X}^*]\Delta t \tag{23}$$

and

$$\boldsymbol{J} = \partial(F[\boldsymbol{X}])/\partial\boldsymbol{X} \tag{24}$$

In the above equations, Δt is the time interval and $\boldsymbol{I}$ is the identity matrix. The matrix $\boldsymbol{J}$ is obtained by expressing Equation (19) in finite difference form and differentiating with respect to the state vector.

The Kalman gain matrix, which defines the relative weighting of model output and measurements, is defined at time step k by:

$$\boldsymbol{G}_k = \boldsymbol{P}_k(-)\boldsymbol{H}_k^{\mathrm{T}}(\hat{\boldsymbol{X}}_k(-))[\boldsymbol{H}_k(\hat{\boldsymbol{X}}_k(-))\boldsymbol{P}_k(-)\boldsymbol{H}_k^{\mathrm{T}}(\hat{\boldsymbol{X}}_k(-)) + \boldsymbol{R}_k]^{-1} \tag{25}$$

where $(-)$ denotes a pre-update quantity, $\hat{\boldsymbol{X}}_k$ is the estimate of the state vector at time step k, and $\boldsymbol{H}$ is the matrix translating state space into observation space:

$$H_{ij}(X_j) = \partial(Z_i)/\partial X_j = \partial(Z_i)/\partial\theta_j \tag{26}$$

$\boldsymbol{H}$ is expressed empirically in a form that represents the dependence of penetration depth $z_{\mathrm{p},i}$ on wavelength and soil moisture content:

$$H_{ij} = c_i e^{-z_j/z_{\mathrm{p},i}} \tag{27}$$

where c_i is the value of H_{ij} at the soil surface ($z = 0$), i is the wavelength index (1 = L-band, 2 = S-band), and j is the soil layer. Based on sensitivity tests with the RTM, we define c_1 and c_2 as:

$$c_1 = 60\theta_1 - 120 \tag{28}$$

$$c_2 = 80\theta_1 - 160 \tag{29}$$

Previous studies indicate that the penetration depth for microwave radiation is proportional to wavelength and inversely related to water content (Jackson and Schmugge, 1989). In this study we define the penetration depth $z_{p,i}$ in terms of wavelength λ_i and the upper layer water content θ_1:

$$z_{p,i} = \lambda_i(0{\cdot}25 - 0{\cdot}20\theta_1) \tag{30}$$

According to Equation (30), the penetration depth approaches $\lambda/4$ for dry soil and $\lambda/20$ when the soil is nearly saturated.

The state vector error covariance matrix $\boldsymbol{P}$ is initialized at time $t = 0$ using estimates of state vector uncertainty and then propagated through time based on the system equations:

$$\mathrm{P}_k(-) = \boldsymbol{\Phi}_{k-1}\boldsymbol{P}_{k-1}\boldsymbol{\Phi}_{k-1}^{\mathrm{T}} + \boldsymbol{Q}_{k-1} \tag{31}$$

in which the subscripts denote time step and $\boldsymbol{Q}$ is the covariance matrix for the model propagation errors. The variance (diagonal) elements of $\boldsymbol{Q}$ are set to a constant value (see Table I) and the covariance (off-diagonal) elements are zero.

When a remote observation is available, the state vector error covariance matrix is updated according to:

$$\boldsymbol{P}_k(+) = [\boldsymbol{I} - \boldsymbol{G}_k\boldsymbol{H}_k(\hat{\boldsymbol{X}}_k(-))]\boldsymbol{P}_k(-) \tag{32}$$

where (+) denotes the post-update estimate.

The state vector (moisture profile) is updated at time step k by applying the Kalman gain $\boldsymbol{G}_k$ to the difference between measured and modelled brightness temperatures:

$$\hat{\boldsymbol{X}}_k(+) = \hat{\boldsymbol{X}}_k(-) + \boldsymbol{G}_k[\boldsymbol{Z}_k - h(\hat{\boldsymbol{X}}_k(-))] \tag{33}$$

where $\hat{\boldsymbol{X}}_k(-)$ is the SHEELS state vector estimate and $h(\hat{\boldsymbol{X}}_k(-))$ is the brightness temperature vector estimated from the radiative transfer model.

Point-scale testing of the Kalman filter

Central Oklahoma has been a focus of extensive hydrological and meteorological research for many years. As a result, there is an abundance of nested measurement networks that make this area uniquely data rich. During SGP97, ground-based microwave brightness temperature measurements were made by the S- and L-band Microwave Radiometer (SLMR), a passive dual-frequency microwave system (Jackson *et al.*, 1997) at the Department of Energy's Atmospheric Radiation Measurement Cloud Atmosphere Radiation Testbed (ARM CART) Central Facility.

As a test of the modelling–remote sensing strategy, we have applied it at point scale using data from SGP97. Implementing the model in this way eliminates issues associated with spatial scaling and provides a means for validating the Kalman update scheme. Data from site CF02 at the Central Facility, where a soil profile station and SLMR were operated, have been used in this test of the Kalman filter algorithm. The study period for this analysis is 23 June–16 July (days 174–197). During this time, the field was covered with senescent wheat that had been cut to a height of about 0·2 m. The modelling system has been applied to simulate conditions within the footprint of SLMR. However, within the footprint the soil moisture measurements were made only for the 0–6 cm layer using a type ML1 ThetaProbe, a manually operated impedance instrument

manufactured by Delta-T Devices, Ltd. The ThetaProbe was inserted vertically into the soil to measure the mean volumetric water content for the 0–6 cm layer. The instrument returns a voltage that is converted to volumetric soil moisture through laboratory calibration. Regression equations ($r = 0{\cdot}995$ or better) were used to convert voltage to volumetric water content. Values used here are the mean of six or nine measurements made within the SLMR footprint area. Because soil moisture and temperature profiles were not measured within the footprint area, observations from the profile station, located in the wheat field approximately 50 m from the footprint area, were used along with the ThetaProbe moisture measurements to provide the required initial conditions for model simulations. The profile data consists of soil moisture at depths of 5, 10, 15, 20, 30 and 40 cm measured with a Campbell Scientific CS615 Water Content Reflectometer (WCR) and temperature at 3, 10, 20 and 40 cm depths obtained using soil thermistors. Measurements taken at the profile site of soil porosity at 5, 15 and 30 cm depths, as well as vegetation water content, were used to supply required model inputs.

Demonstrating the improvements gained by using remote sensing data, even in a local-scale modelling application in which accurate meteorological measurements are used, can be problematic. Even at the local scale, there is a great deal of heterogeneity in surface and sub-surface conditions, especially soil properties. As an example, during SGP97 two soil profile stations were situated approximately 3 m apart at the Central Facility. One was located in a wheat field where the soil had been cultivated, and the second was in a grazed pasture. Following a rainfall of 87 mm, the wetting front penetrated to at least 40 cm depth at the wheat site. In contrast, on the range plot there was no response in soil moisture at the 10 cm depth. The accuracy of soil property measurements is also quite poor. The combination of spatial variability and measurement error has a large impact on the ability to model soil hydrological processes accurately. Finally, models simulate layer-average moisture quantities, whereas *in situ* observations represent conditions at fixed depths. These factors make model-measurement comparisons of soil moisture profiles difficult, especially near the surface, where moisture gradients are large. Remotely sensed data, even those from a ground-based system such as SLMR, are also subject to errors, mainly due to calibration. Consequently, it can be difficult to quantify the benefits of using data assimilation in a hydrologic modelling system.

In an effort to create a robust test of the possible benefit of remote updates, we have performed a series of SHEELS simulations in which errors were intentionally introduced into model rainfall inputs. In each situation, the model was run using the observed meteorology at 30 min time steps until the time of the first available SLMR observation. The modelled moisture and temperature profiles were then used in the RTM to determine the simulated brightness temperature. The Kalman filter [Equation (33)] was applied using simulated and observed brightness temperatures to update the moisture profile estimate; SHEELS was then run until the next update time. SLMR data were used to update the system daily, with the exception of days 177 and 181 when they were unavailable. Updates were performed near 9:00 LDT to maximize data coverage and to avoid the complex moisture and temperature profiles that occur in mid-afternoon due to strong surface heating and drying.

In all simulations, soil properties were based on measured values (Mohanty, 2001) where possible; some values were altered slightly by optimizing the model to the local conditions until good agreement with measured near-surface moisture was attained. Model tuning was limited to the saturated hydraulic conductivity and Clapp–Hornberger parameter, and values were confined to a range consistent with loam soil. Given these constraints, it was not possible to achieve perfect agreement with measurements for the wide range of moisture conditions that occurred during the study. Values of soil and vegetation properties that were not measured were based on Dickinson *et al.* (1993).

The first model runs performed were a SHEELS control run (denoted CON) which used gauge-observed rainfall, and a parallel simulation, CON-U, in which daily SLMR observations were used to update the soil moisture via the Kalman filter algorithm. Figure 2 shows the model soil water content for the 0–6 cm layer (the average of the top three 2 cm layers) for the CON and the CON-U simulations. Also shown in Figure 2 for comparison is the soil moisture measured by the ThetaProbes. Results from the CON simulation match the ThetaProbe measurements closely during the wet periods, but there is a tendency for the upper soil layer in

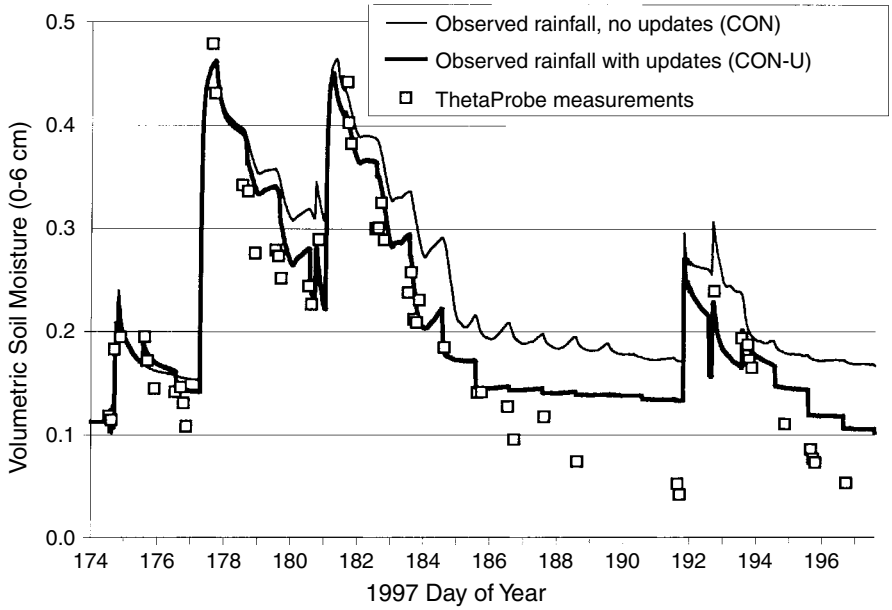

Figure 2. Volumetric soil moisture for the 0–6 cm layer from 'control' simulations using observed rainfall as input. Results from simulations with and without remote updating are shown. Soil moisture measured by the ThetaProbe sensors is shown for comparison

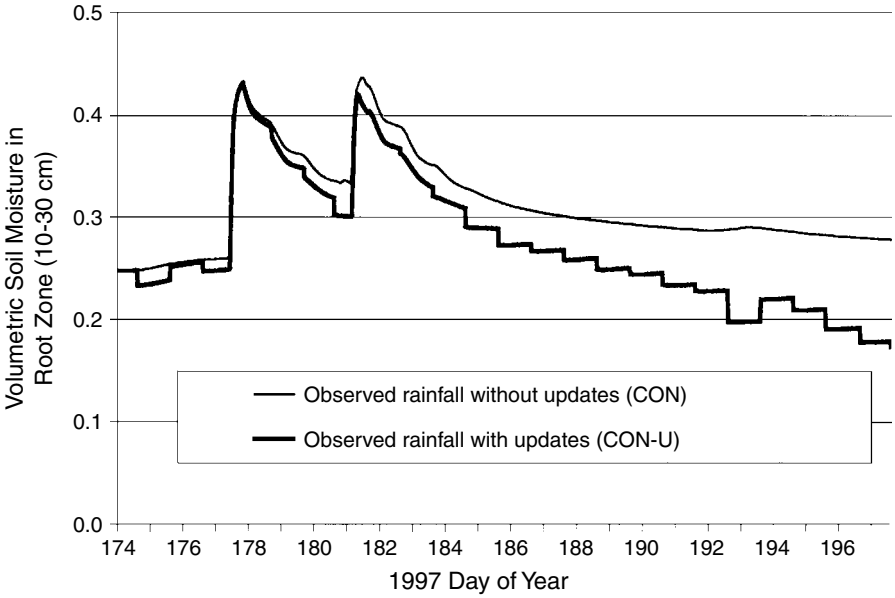

Figure 3. Volumetric soil moisture for the root zone (10–30 cm) from simulations using observed rainfall as input. Model runs with and without remote updating are shown

SHEELS to dry too slowly following the rain events. This is particularly evident during days 186–191, when model estimates are approximately 0·1 m^3 m^{-3} (10% volumetric water content) higher than measurements. Soil moisture updating (CON-U simulation) consistently dries the soil moisture profile relative to CON,

mitigating the noted model bias, but differences remain when the soil is very dry. This is related to the relatively low sensitivity of measured brightness temperature to soil for very dry soil. Root zone (10–30 cm) soil moisture in the CON-U simulation is similarly reduced by Kalman filter updating, as shown in Figure 3.

Two model runs were made to evaluate the effectiveness of the update scheme in the presence of inaccurate precipitation input. These simulations were performed using double and one-half the observed rainfall and are designated DRF and HRF respectively. Parallel runs were also made with Kalman filter updating; we designate these cases DRF-U and HRF-U. Meteorological inputs and initial conditions were based on measurements and were identical for each model run.

The full effect of doubling or halving rainfall input is not always manifested in soil moisture. This is because when rainfall is heavy the additional water reaching the surface may run off, or it may pond and subsequently evaporate without infiltrating. The amounts of precipitation and infiltration for the four rain events for each simulation are shown in Table II. For the smaller rainfall amounts, days 174 and 191–192, virtually all of the water infiltrated in each case. However, for the two larger rainfalls, a considerable amount of water never

Table II. Rainfall amounts for each rain event during the study period, and infiltration amounts for all model simulations. Precipitation amounts for DRF and HRF simulations are respectively double and one-half of the amounts shown

Day of year	Rainfall (mm)	Infiltration (mm)					
		CON	CON-U	DRF	DRF-U	HRF	HRF-U
174	8·6	8·6	8·6	17·2	17·2	4·3	4·3
177	88·9	68·2	69·8	81·2	85·0	43·5	43·6
180–181	53·3	44·8	48·8	46·1	63·2	26·2	26·2
191–192	13·7	13·7	13·7	27·1	27·3	6·8	6·8
Total	164·5	135·3	140·9	172·0	192·8	80·8	80·9

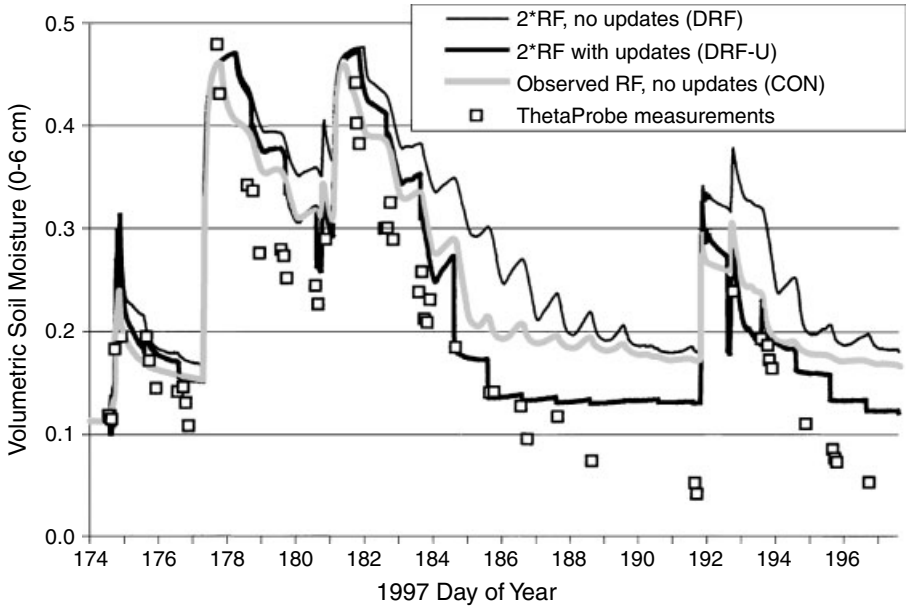

Figure 4. Volumetric soil moisture for the 0–6 cm layer from simulations in which rainfall input is twice the observed amount. Results from simulations with and without remote updating are shown. Control simulation results and soil moisture measured by the ThetaProbe sensors are shown for comparison

entered the soil, especially for the DRF and DRF-U simulations. In fact, for the day 180–181 rainfall there is less infiltration in the DRF case than in CON-U. This is due to wetter antecedent conditions, which result in more ponding and runoff in the DRF simulation. For the entire period, infiltration in the CON, DRF and HRF runs is 82%, 52% and 98% of the imposed rainfall, or 82%, 104% and 49% of the observed rainfall. Thus the infiltration differences, especially between DRF and CON, are much smaller than the imposed rainfall differences.

SHEELS volumetric soil moisture estimates for the 0–6 cm layer and for the root zone (10–30 cm) for the DRF and DRF-U runs are shown in Figures 4 and 5. The output of the control run, which uses observed rainfall, is shown for comparison in both figures, and the ThetaProbe measurements for the surface layer are shown in Figure 4. For the two major rain events on days 177 (89 mm observed) and 180–181 (53 mm), the upper soil layer approached saturation in all cases, so differences between simulations are fairly small immediately after precipitation. However, differences between DRF and CON are quite large during the rapidly drying periods following day 181, reaching a maximum of about 0·1 on day 185. This delayed difference between DRF and CON occurs because the extra rainfall in the DRF simulation is stored in the root zone (note day 182 in Figure 5) and below, providing a moisture source for the upper and root zones during the dry-down period. The differences persist for about 8 days, illustrating the memory of the system to initial soil moisture. During the drying period, updating the soil moisture with the Kalman filter scheme greatly improved the agreement between model 0–6 cm soil moisture and the ThetaProbe measurements. After day 185, the 0–6 cm soil moisture in the DRF-U simulation remains nearly constant, despite the slight downward daily nudging. This is because, in SHEELS, the soil reaches the wilting point and transpiration is greatly reduced thereafter. This behaviour is not observed in the ThetaProbe measurements, which indicate volumetric water contents of less than 5% by day 191. The results shown in Figure 5 show reduced root zone soil moisture in DRF-U relative to DRF, similar to that of the 0–6 cm layer. For both the surface layer and the root zone, the DRF-U soil moistures in the dry-down periods are lower than for the control run, indicating that the update scheme is compensating for the model bias.

Results of runs HRF and HRF-U, in which rainfall input is one-half of the observed amount, are shown for the 0–6 cm layer and the root zone in Figures 6 and 7. As expected, the HRF case underestimates soil

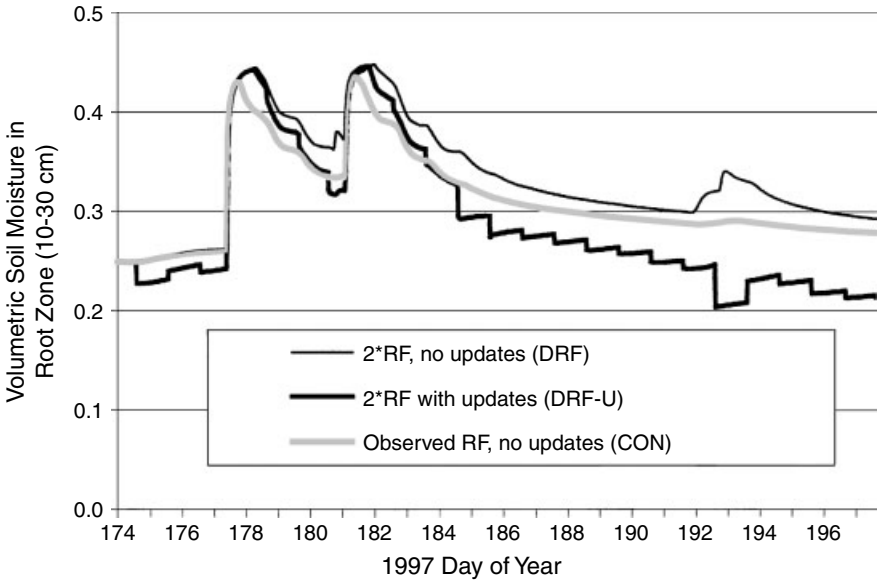

Figure 5. Volumetric soil moisture for the root zone (10–30 cm) from simulations in which rainfall input is twice the observed amount. Model runs with and without remote updating are shown, along with results from the control simulation

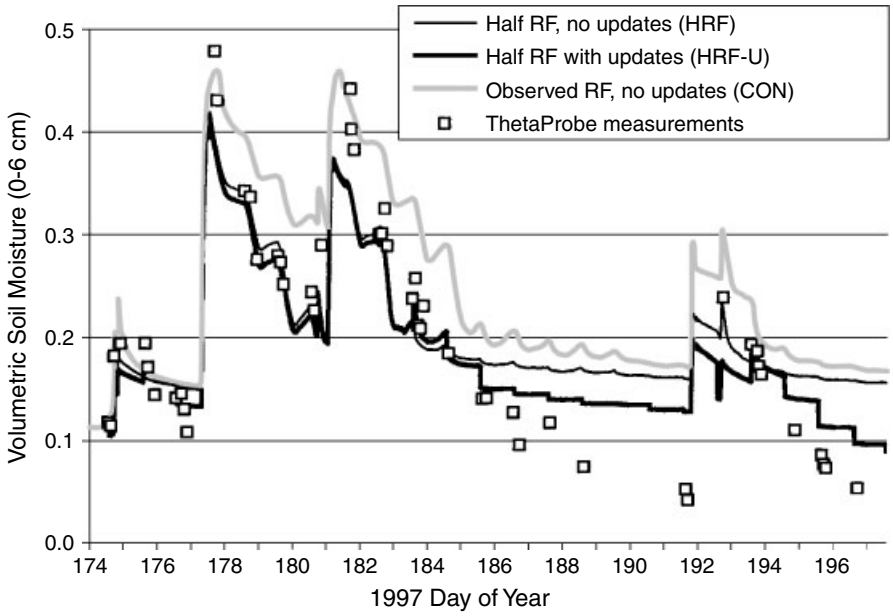

Figure 6. Volumetric soil moisture for the 0–6 cm layer from simulations in which rainfall input is one-half the observed amount. Results from simulations with and without remote updating are shown. Control simulation results and soil moisture measured by the ThetaProbe sensors are shown for comparison

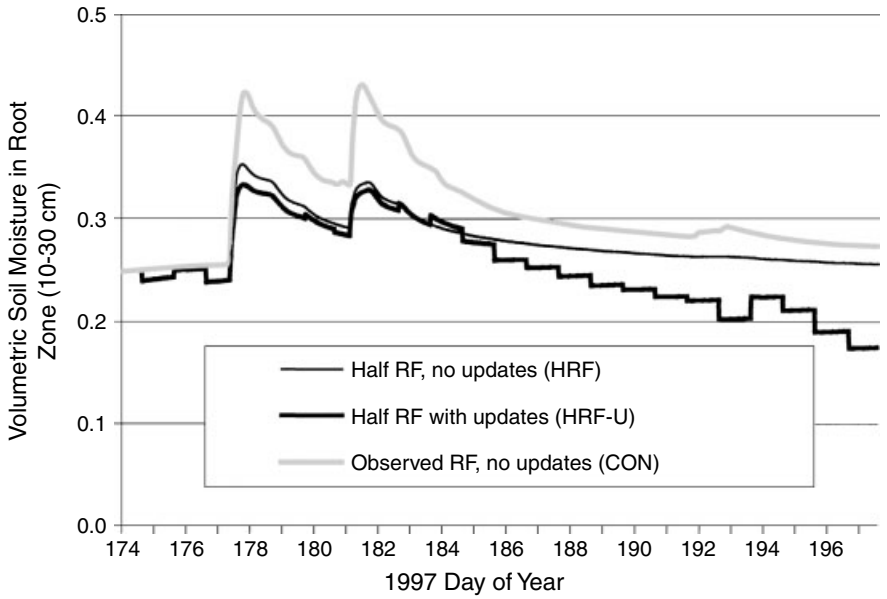

Figure 7. Volumetric soil moisture for the root zone (10–30 cm) from simulations in which rainfall input is one-half the observed amount. Model runs with and without remote updating are shown, along with results from the control simulation

moisture immediately following each rainfall event. However, there is good agreement with the ThetaProbe measurements for several days following the rainfall. Consequently, the updating scheme has little effect on soil moisture before day 185. Because of the model's propensity for limited drying of the 0–6 cm layer, soil

moisture is overestimated during days 185–191. Remote measurements on days 184–190 drive the 0–6 cm soil moisture downward toward the ThetaProbe measurements, although, as in the other cases, there is a limiting value of about 12% Volumetric Soil Moisture. Root zone moisture is also reduced in HRF-U relative to HRF (Figure 7). Similar behaviour is observed in the dry-down during days 192–197, when updating again brings the model soil moisture toward measured values (Figure 6).

In this study, updating of the soil moisture profile was performed on a daily basis. However, in assimilation schemes using satellite data, microwave observations of a particular land area will not be available at such high frequencies in the near future. More realistically, it can be anticipated that measurements will be available every 3 days or so. To illustrate the effects of lower-frequency updating, we repeated the model simulations using updates every 3 days. Results for the 0–6 cm soil layer are shown for the DRF simulations in Figure 8. In the simulations denoted DRF-3U, the first update is applied on day 176. The largest differences between DRF-U and DRF-3U occur on days 180 and 183–184, after rainfall occurred and before the next update in DRF-3U. During the latter period, the benefit of daily updates is apparent, as errors in the DRF-3U simulation become quite large. The update on day 185 results in a very large adjustment in the DRF-3U case, temporarily bringing the results close to observed values. Similar results were observed in the HRF-3U simulations (not shown). In this application, it appears that, in the presence of highly inaccurate rainfall input, applying an assimilation procedure on a 3 day update cycle may result in substantial errors in soil moisture.

Summary and future research

The results shown here are very encouraging. In the presence of highly inaccurate rainfall input, using remote microwave data via a Kalman filter update scheme results in better agreement with observed soil moisture. Without data assimilation, it was seen that model soil moisture for the 0–6 cm layer reached a minimum that was somewhat higher than observed, resulting in substantial errors during the driest part of the study period. Updating the moisture profile daily with remotely sensed brightness temperatures reduced but did not eliminate this bias.

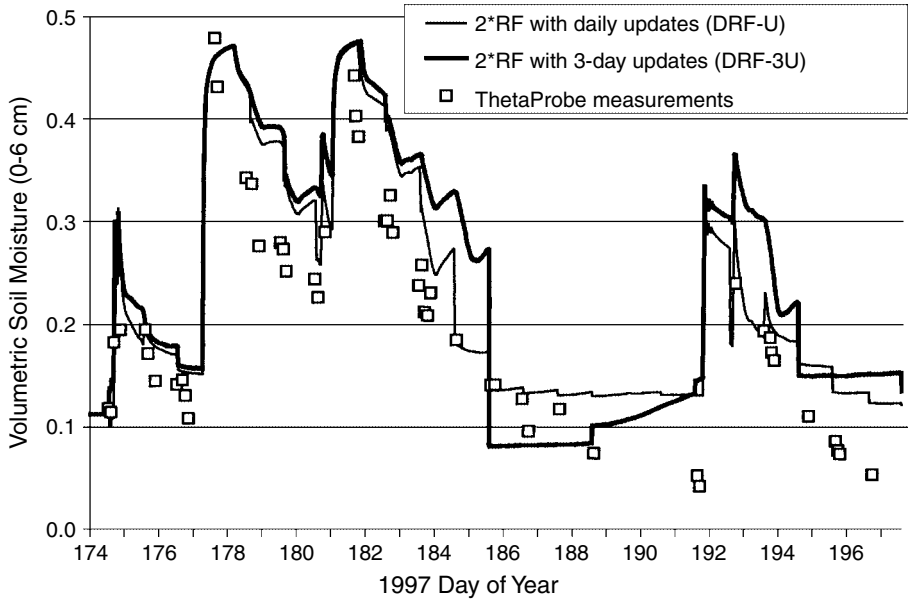

Figure 8. Volumetric soil moisture for the 0–6 cm layer from simulations in which rainfall input is twice the observed amount. Results are shown from simulations in which remote updates are applied at 1 day and 3 day intervals. Soil moisture measured by the ThetaProbe sensors is shown for comparison

The system described here is designed with its ultimate application in mind—operational estimation of near-surface and profile soil moisture using satellite microwave data. Consequently, there are many issues that must be overcome in order to implement this system successfully. Some of these will be addressed in future research which utilizes aircraft data at a relatively small scale, whereas others will become more evident when satellite data are used. The most important of these issues are:

- missing or inaccurate input meteorological data
- long periods of missing remotely sensed data
- effects of scale and surface heterogeneity
- vegetation effects
- agricultural irrigation
- surface roughness
- diurnal effects.

ACKNOWLEDGEMENTS

This work was supported by Universities Space Research Association under NASA Grant NCCW-0084 with Alabama A&M University's HSCaRS Center. We acknowledge Frank Archer, Ahmed Fahsi, Andrew Manu, Jimmy Moore, Narayan Rajbhandari, Garland Robertson, Vishwas Soman, Jacques Surrency, Web Tadesse and Teferi Tsegaye for their assistance during the field experiment. Data were obtained from the Atmospheric Radiation Measurement (ARM) Program sponsored by the US Department of Energy, Office of Energy Research, Office of Health and Environmental Research, Environmental Sciences Division. We also thank Christa Peters-Lidard of Georgia Tech for supplying meteorological data and Dara Entekhabi of the Massachusetts Institute of Technology for many helpful discussions.

REFERENCES

Benard R, Vauclin M, Vidal-Madjar D. 1981. Possible use of active microwave remote sensing data for prediction of regional evaporation by numerical simulation of soil water movement in the unsaturated zone. *Water Resources Research* **17**: 1603–1610.

Brown RG, Hwang PY-C. 1992. *Introduction to Random Signals and Applied Kalman Filtering*. John Wiley and Sons: New York; 502pp.

Capehart WJ, Carlson TN. 1994. Estimating near-surface soil moisture availability using a meteorologically driven soil-water profile model. *Journal of Hydrology* **160**: 1–20.

Choudhury BJ, Schmugge TJ, Chang A, Newton RW. 1979. Effect of surface roughness on the microwave emission from soils. *Journal of Geophysical Research* **84**: 5699–5706.

Clapp RB, Hornberger GM. 1978. Empirical equations for some soil hydraulic properties. *Water Resources Research* **14**: 601–604.

Dickinson RE, Henderson-Sellers A, Kennedy PJ. 1993. *Biosphere Atmosphere Transfer Scheme (BATS) version 1e as coupled to the NCAR Community Climate Model*. NCAR/TN-387 + STR; 72pp.

Dobson MC, Ulaby FT, Hallikainen MT, E1-Rayes MA. 1985. Microwave dielectric behavior of wet soil—part II: dielectric mixing models. *IEEE Transactions on Geoscience and Remote Sensing* **23**: 35–46.

Eagleman JR, Lin WC. 1976. Remote sensing of soil moisture by a 21-cm passive radiometer. *Journal of Geophysical Research* **81**: 3660–3666.

Engman ET, Chauhan N. 1995. Status of microwave soil moisture measurements with remote sensing. *Remote Sensing of the Environment* **51**: 189–198.

Entekhabi D, Nakamura H, Njoku EG. 1994. Solving the inverse problem for soil moisture and temperature profiles by sequential assimilation of multifrequency remotely sensed observations. *IEEE Transactions on Geoscience and Remote Sensing* **32**: 438–448.

Galanatowicz JF, Entekhabi D, Njoku EG. 1999. Tests of sequential data assimilation for retrieving profile soil moisture and temperature from observed L-band radiobrightness. *IEEE Transactions on Geoscience and Remote Sensing* **37**: 1860–1870.

Houser PR, Shuttleworth WJ, Famiglietti JS, Gupta HV, Syed KH, Goodrich DC. 1998. Integration of soil moisture remote sensing and hydrologic modeling using data assimilation. *Water Resources Research* **34**: 3405–3420.

Jackson TJ, Schmugge TJ. 1989. Passive microwave remote sensing system for soil moisture: some supporting research. *IEEE Transactions Geoscience Remote Sensing* **27**: 225–235.

Jackson TJ, Schmugge TJ. 1991. Vegetation effects on the microwave emission of soils. *Remote Sensing of the Environment* **36**: 203–212.

Jackson TJ, Le Vine DM, Swift CT, Schmugge TJ, Schiebe FR. 1995. Large area mapping of soil moisture using the ESTAR passive microwave radiometer in Washita '92. *Remote Sensing of the Environment* **53**: 27–37.

Jackson TJ, O'Neill PE, Swift CT. 1997. Passive microwave observation of diurnal surface soil moisture. *IEEE Transactions on Geoscience and Remote Sensing* **35**: 1210–1222.

Jackson TJ, Le Vine DM, Hsu AY, Oldak A, Starks PJ, Swift CT, Isham JD, Haken M. 1999. Soil moisture mapping at regional scales using microwave radiometry: the Southern Great Plains hydrology experiment. *IEEE Transactions on Geoscience and Remote Sensing* **37**: 2136–2151.

Laymon CA, Manu A, Crosson W, Jackson T. 1999. Defining the range of errors associated with remotely sensed soil moisture estimates. In *Proceedings of SPIE Conference on Earth Surface Remote Sensing*, vol. 3868. September 20–23, Florence, SPIE Press: 504–512.

Li KY, DeJong R, Boisvert JB. 1998. Towards estimating soil moisture in the root zone using remotely sensed surface data. *Canadian Journal of Remote Sensing* **24**: 255–263.

Mohanty BP. 2001. Soil Property Measurement—SGP97, Oklahoma. URL: http://daac.gsfc.nasa.gov/CAMPAIGN_DOCS/SGP97/arssl.html.

Njoku EG, Kong N-A. 1977. Theory for passive microwave remote sensing of near-surface soil moisture. *Journal of Geophysical Research* **82**: 3108–3118.

Prevot L, Bernard R, Taconet O, Vidal-Madjar D, Thony JL. 1984. Evaporation from a bare soil evaluated using a soil water transfer model and remotely sensed surface soil moisture data. *Water Resources Research* **20**: 311–316.

Smith EA, Crosson WL, Cooper HJ, Weng H-Y. 1993. Estimation of surface heat and moisture fluxes over a prairie grassland. Part III: design of a hybrid physical/remote sensing biosphere model. *Journal of Geophysical Research* **98**: 4951–4978.

Smith MR, Newton RW. 1983. *The prediction of root zone soil moisture with a water balance–microwave emission model*. AgRISTAARS Rep. SM-T3-04425.

